IMPROVED QUASI-STATIC METHODS FOR TIME-DEPENDENT NEUTRON DIFFUSION AND IMPLEMENTATION IN RATTLESNAKE

A Thesis

by

ZACHARY M. PRINCE

Submitted to the Office of Graduate and Professional Studies of
Texas A&M University
in partial fulfillment of the requirements for the degree of

MASTER OF SCIENCE

Chair of Committee,	Dr. Jean C. Ragusa
Committee Members,	Dr. Jim E. Morel
	Dr. Bojan Popov
Head of Department,	Dr. Yassin Hassan

May 2017

Major Subject: Nuclear Engineering

ABSTRACT

Going to finish this when I finish the rest of the paper.

DEDICATION

To my mother, my father, my grandfather, and my grandmother. To see what happens with multiple lines, I extend this next part into a second line.

ACKNOWLEDGMENTS

This section is also optional, limited to four pages. It must follow the Dedication Page (or Abstract, if no Dedication). If listing preliminary pages in Table of Contents, include Acknowledgments. Heading (ACKNOWLEDGMENTS) is bold if major headings are bold. It should be in same type size and style as text. So does vertical spacing, paragraph style, and margins. Also, ensure that the spelling of "acknowledgments" matches throughout the text and the table of contents.

I would like to thank the Texas A&M University Office of Graduate and Professional Studies to allow me to construct this LaTeX thesis template. Special thanks to JaeCee Crawford, Amy Motquin, Ashley Schmitt, Rachel Krolczyk, and Roberta Caton for carefully reviewing this material.

CONTRIBUTORS AND FUNDING SOURCES

Contributors

This work was supported by a thesis committee consisting of Professors Jean Ragusa and Jim Morel of the Department of Nuclear Engineering and Professor Bojan Popov of the Department of Mathematics.

All other work conducted for the thesis was completed by the student independently.

Funding Sources

Graduate study was supported by the Endowed Doctoral Fellowship from Texas A&M University, Idaho National Laboratory, and Integrated University Program Fellowship from the Department of Energy.

NOMENCLATURE

TAMU	Texas A&M University
IQS	Improved Quasi-Static Method
INL	Idaho National Laboratory
MOOSE	Multiphysics Object-Oriented Simulation Environment
DOE	Department of Energy
NEAMS	Nuclear Energy Advanced Modeling and Simulation
PRKE	Point Reactor Kinetics Equation
FEM	Finite Element Method
P-C	Predictor-Corrector

TABLE OF CONTENTS

Page

LIST OF FIGURES

FIGURE Page

LIST OF TABLES

TABLE Page

1. INTRODUCTION

Advice: rename through git the files section1 ... with more meaningful filenames, e.g., introduction, theory, ...

Advice: use bibtex for bibliography in the future, rather than bibitem, so that you can change the bibliography style super quickly. Also, most journals provide the bibtex entry for the article, so you just save that in your bib file - yes, no need to type much if you use that feature-

Transient modeling of nuclear reactors has been a chronically foreboding task due to its computationally expensive nature. However, recent developments in nuclear testing this is not the introduction of a short summary, you can spend a bit more time in the topic of transient testing, what is it for, what facilities, how what it simulated before, why a regain of interest in simulation for this today, ... build the storyline..., including the revitalization of the Transient Reactor Testing (TREAT) Facility at Idaho National Laboratory (INL), have brought significant attention to the development of transient reactor modeling. 3-D transient computational methods currently in use at national laboratories, including INL, have proven to be overbearingly computationally expensive for complex, real-world scenarios. Therefore, implementation of more efficient and faster methods for 3-D transient simulations is highly desired this was already a problem when Karl Ott introduced IQS in 1977(?) so to rationale sounds a bit hollow the way you present it and yet we are doing it and Downar was awarded last year a grant to do this too. I think the real reason is that most modern reactor physics tools have not being used much for fast transients, so the only thing we are doing is bringing back the method into modern tools. However, in doing so, . The Department of Energy (DOE), through its NEAMS (Nuclear Energy Advanced Modeling and Simulation) program, has especially sought the development of transient multiphysics

capability in INL's MOOSE (Multiphysics Object-Oriented Simulation Environment).

I think an outline for the introduction should be

1. reactor transient testing. Background, etc... this subsection should conclude on the overarching need of transient testing: computational methods for multiphysics reactor transients. It should also introduce the next 2 subsections, which are both about lit review, one on time-dependent neutronics, one on multiphysics solution techniques for reactor physics.

2. literature review on mostly neutronics time dependent: challenges in computational methods for time-dependent neutron balance equations. the size of the phase-space, the need for implicitness in the temporal treatment due to the stiffness, ... this should open up to a discussion on alternate methods, such as IQS, ... it is a lit review, so no need for equations, but rather a demonstration that you know the background and have a solid understand of that foundation to lay the ground from your OWN work. As part of this lit, some discussion of Mund's, Dulla's, Ott's, Monier,'s the Canadian's papers is welcome.

3. now, reactor transients also means coupled to other physics. this is were you discuss some aspect related to multiphysics. you can start with the general discussion that this is typically a nonlinear problem, that it can be solved via picard or newton. this is maybe a segway into a discussion/introduction about MOOSE. Then you go back on IQS and add the multiphysics aspects. Ott did some work with multiphysics, I gave you the code manual of his own software where he discusses when he decided to do shape updates.

Generally speaking, the rest is real good but you need to spend some time on these 5-8 pages of introduction that set the tone and the background. Everybody needs to understand

that you know a lot; that your thoughts are well organized and clear; the rest will come easy (except some results ...).

side note: we need to put the small results about sdirk being poor for stiffness problem. maybe as an appendix. I want to keep that knowledge somewhere. MOOSE is a multi-physics framework being developed at INL that presents the architecture for physics-based applications [1]. Rattlesnake is a large application in MOOSE that involves deterministic radiation transport physics. Currently, Rattlesnake is able to solve steady-state, transient, and k-eigenvalue neutron transport and diffusion problems using finite element methods (FEM) [2].

The difficulty in transient reactor modeling is due to

1. the high-dimensionality of the phase-space for the governing equations that describe the flux of neutrons (6-D+time for multigroup neutron transport and 4-D+time for multigroup neutron diffusion), and

2. the fact that the time discretization has to be implicit, which leads to stiff system of equations.

The transport equation has seven independent variables: space ($\vec{r}$), energy (E), direction ($\vec{\Omega}$), and time (t) [3]. Nuclear reactor simulations often utilize the neutron diffusion approximation, which carefully eliminates the dependence on direction. For the purpose of this research, neutron diffusion will be discussed exclusively.

1.1 Neutron Diffusion Solution Process

For computational purposes, the neutron diffusion equation is discretized in space, energy, and time. There are several viable discretization schemes for each of these vari-

ables; FEM for space and multigroup in energy are used for the development of this research. Since the purpose of this research involves temporal dependence, discretization in time was kept general. The time dependent neutron diffusion equation with delayed neutron precursors can be seen in Equations 1.1a and 1.1b.

$$\frac{1}{v^g}\frac{\partial \phi^g}{\partial t} = \frac{\chi_p^g}{k_{\mathit{eff}}}(1-\beta)\sum_{g'=1}^{G}\nu^{g'}\Sigma_f^{g'}\phi^{g'} + \sum_{g'\neq g}^{G}\Sigma_s^{g'\to g}\phi^{g'} + \sum_{i=1}^{I}\chi_{d,i}^g\lambda_i C_i - \left(-\nabla\cdot D^g\nabla + \Sigma_r^g\right)\phi^g\,, \quad 1\leq g\leq G \tag{1.1a}$$

$$\frac{dC_i}{dt} = \frac{\beta_i}{k_{\mathit{eff}}}\sum_{g=1}^{G}\nu^g\Sigma_f^g\phi^g - \lambda_i C_i\,, \quad 1\leq i\leq I \tag{1.1b}$$

where,

ϕ^g = Scalar flux in energy group g

C_i = Concentration of delayed neutron precursor i

Σ_f^g = Fission cross section in energy group g

Σ_r^g = Removal cross section in energy group g

$\Sigma_s^{g' \to g}$ = Scattering cross section from energy group g' to g

v^g = Neutron velocity in energy group g

χ_p^g = Fission spectrum of prompt neutrons

$\chi_{d,i}^g$ = Fission spectrum of delayed neutrons from precursor i

ν^g = Total number of neutrons per fission

D^g = Diffusion coefficient in energy group g

λ_i = Decay constant of precursor i

β_i = Delayed neutron fraction from precursor i

β = Total delayed neutron fraction ($\beta = \sum_{i=1}^{I} \beta_i$)

Most reactor computation frameworks, including Rattlesnake, discretize the time variable directly with these equations using a multitude of schemes (Implicit Euler, Crank-Nicholson, implicit Runge-Kutta, etc.). In this paper, the method of discretizing Equations 1.1a and 1.1b is generally referred to as "implicit discretization". This research intends to improve upon this method by instead implementing the improved quasi-static method (IQS) for neutron kinetics and implement it within a multiphysics setting.

1.1.1 Point Reactor Kinetics Equation

A common solution process for neutron kinetics is the evaluation of the point reactor kinetics equation (PRKE). The derivation of this equation involves factorization flux into a space-dependent shape and time-dependent amplitude. This factorization immedi-

ately creates a large assumption that the spacial variance of the flux is time-independent. However, this takes very little computational effort to evaluate because the multitudinous variables from the spacial discretization only needs to be evaluated on the initial time step. The rest of the time steps only evaluated one variable: amplitude.

1.1.2 Improved Quasi-Static Method

IQS is a spatial kinetics method that involves factorizing the flux solution into space- and time-dependent components [4, 5]. These components are the flux's amplitude and its shape. Amplitude is only time-dependent, while the shape is both space- and time-dependent. However, the impetus of the method is the assumption that the shape is only weakly dependent on time; therefore, the shape may not require an update at the same frequency as the amplitude function, but only on larger macro-time steps.

Since shape and amplitude share a independent variable, they are temporally coupled. Additionally, the resulting system of equations is heavily nonlinear. The are a number of published strategies that evaluate this system, but a in depth comparison of the techniques has not been found.

1.2 Objective

The goal of this research is to continue the investigation and development of the improved quasi-static method. This goal requires the development of IQS in a easily modifiable, prototype-like code, as well as a robust FEM framework.

The prototyping code is used to investigate time discretization and nonlinear iteration schemes. The prototype will also guide the development of IQS in the large FEM framework of Rattlesnake/MOOSE, where more complex examples and benchmarks can be tested. Development in Rattlesnake also spawns the opportunity to test IQS with multiphysics, namely temperature feedback, and time adaptation.

2. Improved Quasi-Static Method

2.1 Theory

IQS involves factorizing the flux from Equation (1.1a) into time-dependent amplitude (p) and space- and time- dependent shape (φ). The resulting equation is the shape-diffusion equation with precursors represented by Equations 2.1a and 2.1b.

$$\begin{aligned}\frac{1}{v^g}\frac{\partial \varphi^g}{\partial t} =& \frac{\chi_p^g}{k_{eff}}(1-\beta)\sum_{g'=1}^{G}\nu^{g'}\Sigma_f^{g'}\varphi^{g'} + \sum_{g'\neq g}^{G}\Sigma_s^{g'\to g}\varphi^{g'} \\ &- \left(-\nabla\cdot D^g\nabla + \Sigma_r^g + \boxed{\frac{1}{v^g}\frac{1}{p}\frac{dp}{dt}}\right)\varphi^g + \boxed{\frac{1}{p}}\sum_{i=1}^{I}\chi_{d,i}^g\lambda_i C_i, \quad 1\leq g\leq G\end{aligned} \tag{2.1a}$$

$$\frac{dC_i}{dt} = \frac{\beta_i}{k_{eff}}\boxed{p}\sum_{g=1}^{G}\nu^g\Sigma_f^g\varphi^g - \lambda_i C_i\,, \quad 1\leq i\leq I \tag{2.1b}$$

We note that the time-dependent shape equation is similar to the time-dependent flux equation, with the following modifications:

1. The shape equation contains an additional term equivalent to a removal cross section, $\frac{1}{v^g}\frac{1}{p}\frac{dp}{dt}$.
2. The delayed neutron source term is divided by p.
3. The system of equations is now nonlinear due to the factorization.
4. An equation is needed to obtain the amplitude p.

To derive the amplitude equation, the shape/precursors equations are weighted by a space-dependent function and integrated over the phase-space. The weight function is

typically the adjoint flux ϕ^{*g}, which can be proven to minimize truncation error [3]. The final expressions are given below:

$$\frac{dp}{dt} = \left[\frac{\rho - \bar{\beta}}{\Lambda}\right] p + \sum_{i=1}^{I} \bar{\lambda}_i \xi_i \tag{2.2a}$$

$$\frac{d\xi_i}{dt} = \frac{\bar{\beta}_i}{\Lambda} - \bar{\lambda}_i \xi_i \quad 1 \leq i \leq I \tag{2.2b}$$

This equation is also known as the point reactor kinetics equation (PRKE); where the reactivity, effective delayed-neutron fraction, and delayed-neutron precursor decay constant are defined as follows:

$$\frac{\rho - \bar{\beta}}{\Lambda} = \frac{\sum_{g=1}^{G} \left(\phi^{*g}, \frac{\chi_p^g}{k_{eff}} (1-\beta) \sum_{g'=1}^{G} \nu^{g'} \Sigma_f^{g'} \varphi^{g'} + \sum_{g' \neq g}^{G} \Sigma_s^{g' \to g} \varphi^{g'} - \left(-\nabla \cdot D^g \nabla + \Sigma_r^g\right) \varphi^g \right)}{\sum_{g=1}^{G} \left(\phi^{*g}, \frac{1}{v^g} \varphi^g \right)} \tag{2.3a}$$

$$\frac{\bar{\beta}}{\Lambda} = \sum_{i=1}^{I} \frac{\bar{\beta}_i}{\Lambda} = \sum_{i=1}^{I} \frac{1}{k_{eff}} \frac{\sum_{g=1}^{G} (\phi^{*g}, \chi_{d,i}^g \beta_i \sum_{g'=1}^{G} \nu^{g'} \Sigma_f^{g'} \varphi^{g'})}{\sum_{g=1}^{G} \left(\phi^{*g}, \frac{1}{v^g} \varphi^g \right)} \tag{2.3b}$$

$$\bar{\lambda}_i = \frac{\sum_{g=1}^{G} (\phi^{*g}, \chi_{d,i}^g \lambda_i C_i)}{\sum_{g=1}^{G} (\phi^{*g}, \chi_{d,i}^g C_i)} \tag{2.3c}$$

The following inner product definition has been used: $(\phi^{*g}, f) := \int_D \phi^{*g}(\vec{r}) f(\vec{r}) d^3 r$.

Additionally, in order to impose uniqueness on the factorization and to derive the PRKE, the following normalization condition is imposed: $\sum_{g=1}^{G} \left(\phi^{*g}, \frac{1}{v^g} \varphi^g \right) = \textit{constant}$ [5].

Solving for the shape in Equation (2.1a) can become expensive, especially in two or three dimensions, and even more so when using the transport equations in lieu of the diffusion equations. Using IQS, one expects the time dependence of the shape to be weaker than that of the flux itself, thus allowing for larger time step sizes in updating the shape.

The PRKE equations form a small ODE system and can be solved using a much smaller time step size. In transients where the shape varies much less than the flux, IQS can thus be very computationally effective. The two-time scale solution process, a micro scale for the PRKE and a macro scale for the shape, is illustrated in Figure 2.1.

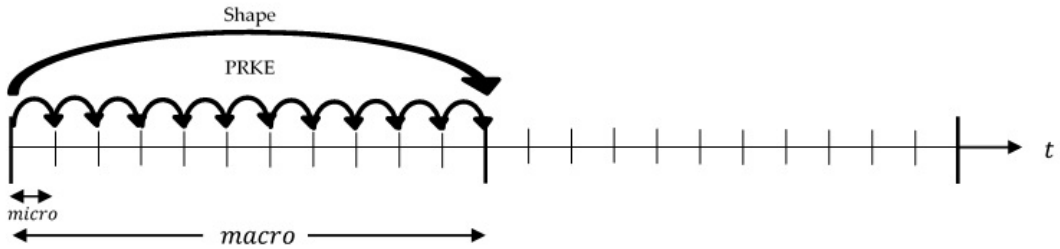

Figure 2.1: IQS method visualization

2.1.1 Operator Notation and Extension of IQS to Multigroup Transport Equations

For simplicity, the previous section only described the IQS implementation using the neutron diffusion equation. However, deriving the IQS form for other neutron balance equations (e.g., transport, simplified transport, etc.) is very similar. To this end, we re-write the neutron conservation equations in operator form, shown in Equation (2.4).

$$\frac{\partial}{\partial t}\left(\frac{\Psi^g}{v^g}\right) = \sum_{g'}\left(H^{g'\to g} + P_p^{g'\to g}\right)\Psi^{g'} - L^g\Psi^g + S_d^g \tag{2.4}$$

where Ψ^g is the multigroup neutron flux (angular flux in the case of transport), $H^{g'\to g}$ is the scattering operator, $P_p^{g'\to g}$ is the prompt neutron production operator, L^g is the loss operator, and S_d^g is the delayed neutron source operator. Using Equation (1.1a), the reader may easily obtain the functional form for these operators in the case of a diffusion approximation. Next, the factorization $\Psi^g(\vec{r},\vec{\Omega},t) = p(t)\psi^g(\vec{r},\vec{\Omega},t)$ is introduced, where the

shape is denoted by ψ^g, leading to the following shape equations, Equation (2.5):

$$\frac{\partial}{\partial t}\left(\frac{\psi^g}{v^g}\right) = \sum_{g'}\left(H^{g'\to g} + P_p^{g'\to g}\right)\psi^{g'} - \left(L^g + \frac{1}{v^g}\frac{1}{p}\frac{dp}{dt}\right)\psi^g + \frac{1}{p}S_d^g \tag{2.5}$$

Finally, the PRKE parameters are defined by Equations 2.6 and 2.7, where $(\Psi^{*g}, f^g) = \int_{4\pi}\int_D \Psi^{*g}(\vec{r},\vec{\Omega})f^g(\vec{r},\vec{\Omega})d^3r d^2\Omega$.

$$\frac{\rho - \bar{\beta}}{\Lambda} = \frac{\sum_{g=1}^G \left(\Psi^{*g}, \sum_{g'}(H^{g'\to g}g + P_p^{g'\to g} - L^{g'}\delta_{g'g})\psi^{g'}\right)}{\sum_{g=1}^G \left(\Psi^{*g}, \frac{1}{v^g}\psi^g\right)} \tag{2.6}$$

$$\frac{\bar{\beta}}{\Lambda} = \sum_{i=1}^I \frac{\bar{\beta}_i}{\Lambda} = \sum_{i=1}^I \frac{\sum_{g=1}^G (\Psi^{*g}, \sum_{g'} P_{d,i}^{g'\to g}\psi^{g'})}{\sum_{g=1}^G \left(\Psi^{*g}, \frac{1}{v^g}\psi^g\right)} \tag{2.7}$$

where $P_{d,i}^{g'\to g}$ is the delayed-neutron operator for precursor group i.

This section is simply meant to show the theoretical expandability of IQS to transport problems and its derivation in operator notation. As stated previously, this research only applies and tests IQS with diffusion problems.

2.2 Iterative Solution Techniques

As we noted in Section 2.1, shape-PRKE equations are a nonlinear system and thus may be solved in a iterative manner. Each macro time step can be iterated so the best shape is used to compute power at the micro time steps. Sissaoui et al. from [6], Koclas et al. from [7], Devooght et al. from [8], and Monier from [9] all use iterative techniques for their quasi-static simulations. They all undergo a similar process:

Step 1: Compute the PRKE parameters at the end of the macro step using the last computed shape

Step 2: Linearly interpolate the computed PRKE parameters over the macro step

Step 3: Solve the PRKE on micro steps over the entire macro step

Step 4: Solve the shape equation on the macro step using the computed values of p and dp/dt.

Step 5: Check if the shape solution has converged:

- *No:* Repeat the same macro time step
- *Yes:* Move on to the next macro time step

This process can be visualized by Figure 2.2.

The major difference between the methods of these authors is the convergence criteria used. Sissaoui and Koclas [6, 7] use fixed point iteration where the criteria is the simply the normalized difference between the last two computed shapes. Monier in [9] also does fixed point iterations with the same criteria, except the solution is scaled by $\frac{\sum_{g=1}^{G}\left(\phi^{*g},\frac{1}{v^g}\varphi^g(t_n)\right)}{\sum_{g=1}^{G}\left(\phi^{*g},\frac{1}{v^g}\varphi^g(t_{n+1})\right)}$ after each iteration. Devooght in [8] does a Newton-SOR iteration where the residual of the shape function evaluation is the convergence criteria and next iteration's solution is computed using Newton-Raphson method.

These techniques are by no means an exhaustive list of the possible iteration techniques for IQS. Dulla et al. in [5] does an in depth analysis of the fixed point iteration technique most similar to Sissaoui and Koclas, involving convergence rates and solution results. However, no comprehensive analysis of iteration techniques exists, comparing both Newton and fixed-point convergence rates. The following sections describes each iteration technique investigated by this research.

2.2.1 Shape Convergence

The most obvious convergence criteria is to observe the change in the shape from one iteration to the next. Monier in [9] observes the L^∞ norm of the shape for the convergence

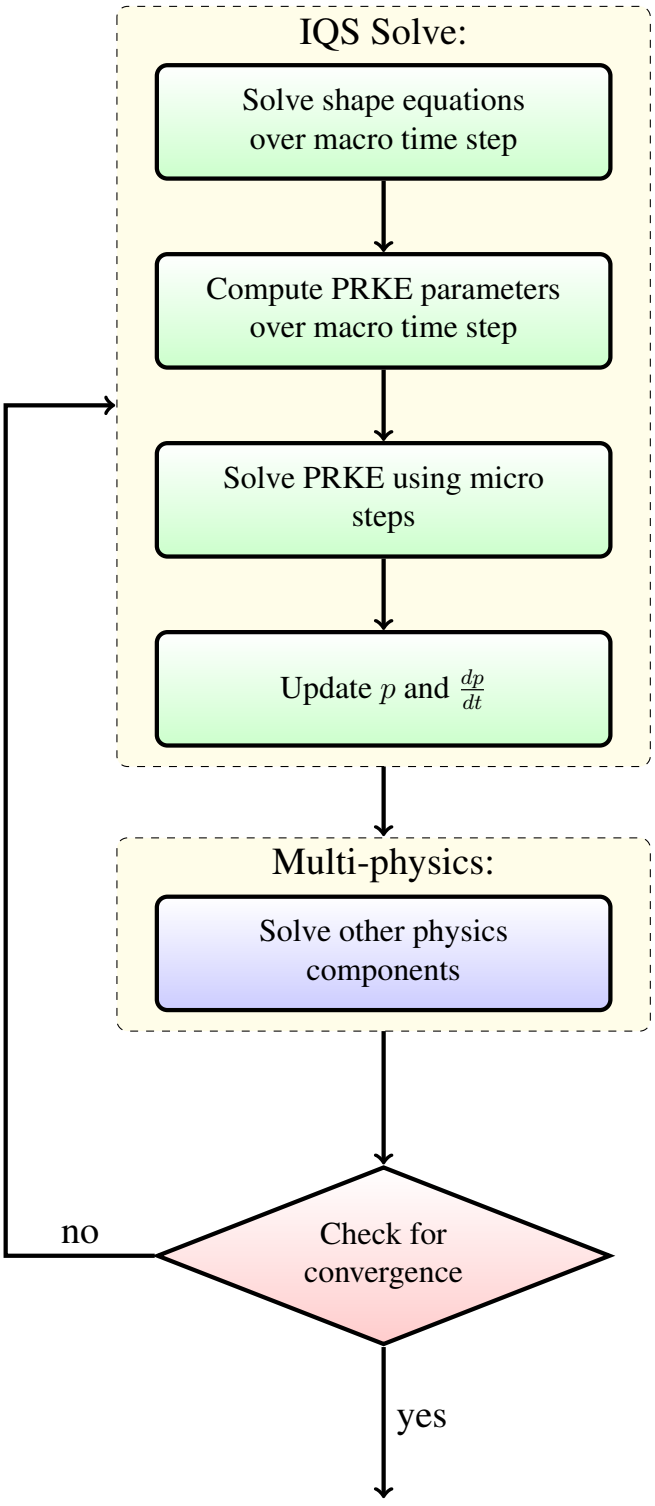

Figure 2.2: Visualization of IQS fixed-point iteration process

criteria, described in Equation (2.8). However, any norm can be used for the criteria, so a L^2 norm is another possible criteria, described by Equation (2.9).

$$\frac{\max\left|\varphi_n^{(k+1)} - \varphi_n^{(k)}\right|}{\max\left|\varphi_n^{(k+1)}\right|} < \epsilon_\varphi \tag{2.8}$$

$$\frac{\left\|\varphi_n^{(k+1)} - \varphi_n^{(k)}\right\|_{L^2}}{\left\|\varphi_n^{(k+1)}\right\|_{L^2}} < \epsilon_\varphi \tag{2.9}$$

Where n is the time step, k is the iteration number, and ϵ_φ is the numerical criteria provided by a user. There is no guarantee that the shape converges, so max number of iterations is typically enforced.

2.2.2 Property Convergence

Monier in [9] describes other properties, other than shape, to observe for convergence, shown in Equations (2.10) - (2.12). These criteria can be added constraints to Equation (2.8) or be in supplement to.

$$\left(\frac{\rho}{\Lambda}\right)^{(k+1)} - \left(\frac{\rho}{\Lambda}\right)^{(k)} < \epsilon_\rho \tag{2.10}$$

$$p_n^{k+1} - p_n^k < \epsilon_p \tag{2.11}$$

$$\frac{K_n^{(k+1)} - K_0}{K_0} < \epsilon_K \tag{2.12}$$

Where K is the IQS uniqueness expression:

$$K_n^{(k+1)} = \sum_{g=1}^{G}\left(\phi^{*g}, \frac{1}{v^g}\varphi_n^{g,(k+1)}\right) \tag{2.13}$$

ϵ_ρ is the reactivity convergence criteria, ϵ_p is the amplitude convergence criteria, and

ϵ_K is the constraint convergence criteria.

2.2.3 Solution Scaling

In order to preserve the uniqueness criteria, it is beneficial to scale the shape such that the K_n is constant, shown in Equation (2.14). This scaling can also be done after each iteration, to insure that the uniqueness criteria is satisfied whenever the shape is evaluated.

$$\varphi_n^g = \varphi_n^{g,(\text{last})} \frac{K_0}{K_n^{(\text{last})}} \tag{2.14}$$

2.2.4 Preconditioned Jacobian-Free Newton-Krylov

By far, the most common nonlinear system iteration method in MOOSE is Preconditioned Jacobian-Free Newton-Krylov with Generalized Minimal RESidual method (GMRES) as the linear system solver. This section only descirbes the methods' application to IQS; a very detailed description of PJFNK is transcribed by Knoll in [10]. Essentially, the IQS system of equations can be described by Equation (2.15). Where A is a matrix operator, φ is the solution vector, and F is the forcing vector.

$$A(\varphi(p))\varphi = F(\varphi, p, t) \tag{2.15}$$

Applying the residual based Newton-method yields:

$$J\delta\varphi = -R(\varphi, p) \tag{2.16}$$

Where J is the Jacobian matrix defined as $J_{ij} = \partial R_i / \partial \varphi_j$, $\delta\varphi$ is the error in the iterating solution, and R is the residual vector defined as $A\varphi - F$ (most methods simply define the residual instead of evaluating this expression). For IQS, a residual evaluation entails a PRKE parameter evaluation and the PRKE evaluation over the entire macro-step. Apply-

ing a preconditioner P yields:

$$(JP^{-1})(P\delta\varphi) = -R(\varphi, p) \tag{2.17}$$

This resulting system can be split into two systems, represented by Equations (2.18) and (2.19).

$$(JP^{-1})w = -R(\varphi, p) \tag{2.18}$$

$$\delta\varphi = P^{-1}w \tag{2.19}$$

Solving Equation (2.18) requires the evaluation of Jacobian operator, which is done each GMRES iteration in two steps:

1. Approximately solve the preconditioner system for y: $Py = w$
2. Perform matrix-free Jacobian operation: $Jy \approx [R(\varphi + \epsilon y, p') - R(\varphi, p)]/\epsilon$

This Jacobian operation is a finite difference approach. ϵ is a perturbation scalar and p' is the amplitude computed with PRKE parameters calculated from the perturbed shape. For IQS, the PRKE and its parameters must be evaluated for the perturbed and original system, although the unperturbed residual is stored from the beginning of the PJFNK iteration.

2.3 Predictor-Corrector version of IQS (IQS P-C)

The Predictor-Corrector (P-C) version of IQS factorizes the flux and derives the PRKE the same way as the standard version, but the solution of the coupled system of equations is different. In the IQS P-C version, the flux equations (not the shape equations) are solved (represented by Equations 1.1a and 1.1b) in order to obtain a predicted flux

solution. This predicted flux is then converted to a shape by rescaling it as follows:

$$\varphi_{n+1}^{g} = \underbrace{\phi_{n+1}^{g}}_{\text{predicted}} \frac{K_0}{K_{n+1}} \tag{2.20}$$

where the scaling factors are given by

$$K_{n+1} = \sum_{g=1}^{G} \left(\phi^{*g}, \frac{1}{v^g} \phi_{n+1}^{g} \right) \tag{2.21}$$

$$K_0 = \sum_{g=1}^{G} \left(\phi^{*g}, \frac{1}{v^g} \varphi_{n+1}^{g} \right) = \sum_{g=1}^{G} \left(\phi^{*g}, \frac{1}{v^g} \phi_{0}^{g} \right) \tag{2.22}$$

The PRKE parameters are then computed with this shape using Equations 2.3a - 2.3c and interpolated over the macro step, then the PRKE ODE system is solved on the micro time scale. With the newly computed amplitude, the shape is rescaled into a flux and the final corrected flux is given by:

$$\underbrace{\phi_{n+1}^{g}}_{\text{corrected}} = p_{n+1} \times \varphi_{n+1}^{g} \,. \tag{2.23}$$

The advantage to the predictor-corrector method is there is no iteration necessary for this method and, in turn, is much simpler and faster than the standard IQS. Ikeda et al. in [11] and Goluoglu et al. in [12] both use IQS P-C for complex, three-dimensional problems. Their results prove IQS P-C to be impressively effective, despite the de-coupling of the system. Dulla et al. in [5] also describes an in depth comparison of IQS P-C with traditional IQS.

2.4 Temperature Feedback

IQS is first and foremost a nuclear reactor simulation method. In nuclear reactors, multiple physics affect the profile of the neutron flux. The most simple example of mulit-

physics reactor simulations is adiabatic heat up with Doppler feedback. The principle of Doppler feedback is that fission in a fuel causes the material to increase temperature and induces a change in the neutronics properties. The material heat up is described by Equation (2.24); where ρ is the material density, c_p is the specific heat, T is temperature, and κ_f is the energy released per fission [13]. The change in temperature of the material mainly affects the thermal macroscopic absorption cross section described by Equation (2.25) [13].

$$\rho c_p \frac{\partial T(\vec{r},t)}{\partial t} = \kappa_f \sum_{g=1}^{G} \Sigma_f^g \phi^g(\vec{r},t) \tag{2.24}$$

$$\Sigma_a^{thermal}(\vec{r},t) = \Sigma_a^{thermal}(\vec{r},0)\left[1+\gamma\left(\sqrt{T}-\sqrt{T_0}\right)\right] \tag{2.25}$$

2.4.1 Temperature Evaluation

Temperature evaluation (Equation (2.24)) is quite similar to the evaluation of the delayed neutron precursors from Section 2.6. A typical implicit solver would simply use the interpolated flux at end of the temperature time step for the right hand side of the equation, a theta-method discretization. However, IQS has much more information about the profile of the flux along the time step because of the micro-step amplitude evaluation. Therefore, it is possible to solve for temperature using a semi-analytical approach, shown by Equation (2.26).

$$T^{n+1} = T^n + \frac{\kappa_f}{\rho c_p}\left(a_2\varphi^{n+1} + a_1\varphi^n\right) \tag{2.26}$$

Where n corresponds to the beginning of the temperature step. a_1 and a_2 are integration coefficients defined by Equation (2.27) and Equation (2.28). Any interpolation of the amplitude along the micro steps is possible for the integration, this application uses piece-

wise linear.

$$a_1 = \int_{t_n}^{t_{n+1}} \left(\frac{t_{n+1} - t'}{\Delta t} \right) p(t') dt' \tag{2.27}$$

$$a_2 = \int_{t_n}^{t_{n+1}} \left(\frac{t' - t_n}{\Delta t} \right) p(t') dt' \tag{2.28}$$

2.4.2 Intermediate Time Scale

For IQS, this temperature feedback affects both the shape equation and the reactivity of the PRKE; thus, it is an additional nonlinear component to the already coupled shape-amplitude equations. In foresight to the application of this component, temperature is much more time dependent than the shape, but less so than the amplitude. Therefore, the evaluation of temperature will have its own time scale. A possible solution process for a problem with temperature feedback will have time three time scales portrayed in Figure 2.3. The first time scale is the shape solve, the second is the temperature evaluation as well as the computation of PRKE parameters, and the third is the PRKE scale. It is important to note that the number of time steps in each scale is arbitrary and meant only for visual purposes.

2.4.3 Programming Logic

The couplings between temperature, amplitude, and shape are all nonlinear, so iteration processes are needed for each time scale. The amplitude and temperature need to be iterated on the middle time scale until convergence on each temperature step. Then another iterative process needs to occur in the shape time scale on all three variables. Figure 2.4 shows the programming diagram implement to execute this process. The time increment of $\Delta t/3$ for the temperature solve is arbitrary and is meant only to match Figure 2.3.

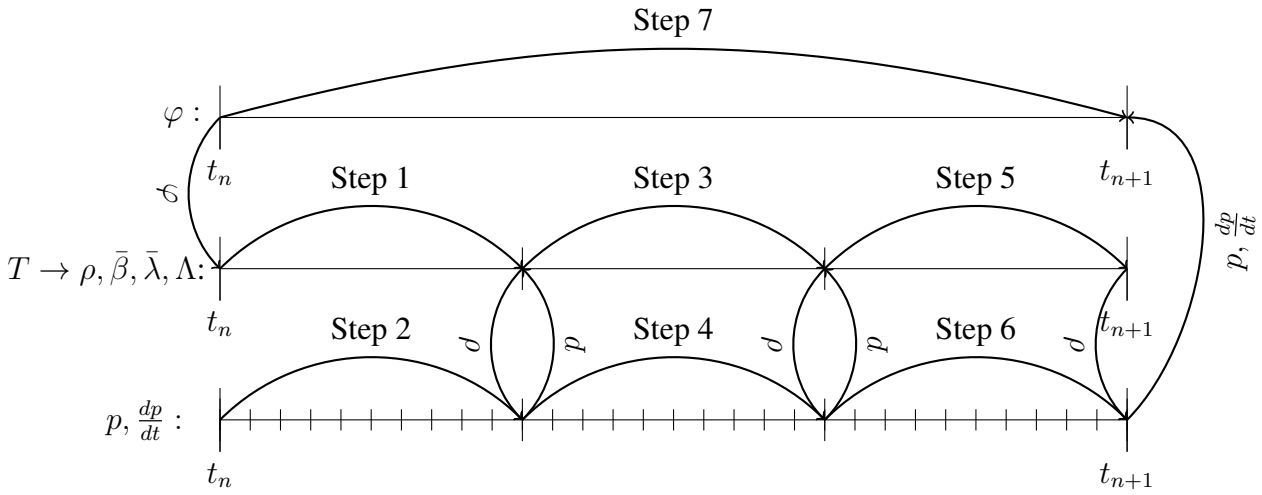

Figure 2.3: Time scales and process of IQS with temperature feedback

2.5 Time Discretization Schemes

A vital part of the verification and validation for IQS is analyzing error convergence. Since any time discretization scheme is capable of being applied to the shape equation of IQS, it is important to investigate IQS's performance to a variety of these schemes. There is lack of literature that applies IQS to schemes other than implicit Euler; higher order schemes are never rigorously tested. This research intends to apply a variety of schemes, including implicit Euler, Crank-Nicholson, backward difference formula (BDF), and diagonally implicit Runge-Kutta (DIRK), to test stability and error convergence. For brevity in the following sections, the shape-diffusion equation is represented by a general operator notation, described by Equation (2.29).

$$IV\frac{\partial\varphi}{\partial t} = A\varphi + b \tag{2.29}$$

Where IV is the inverse velocity operator, A contains all the operations on φ from the left-hand-side of Equation (2.1a), and b is the source from the precursors.

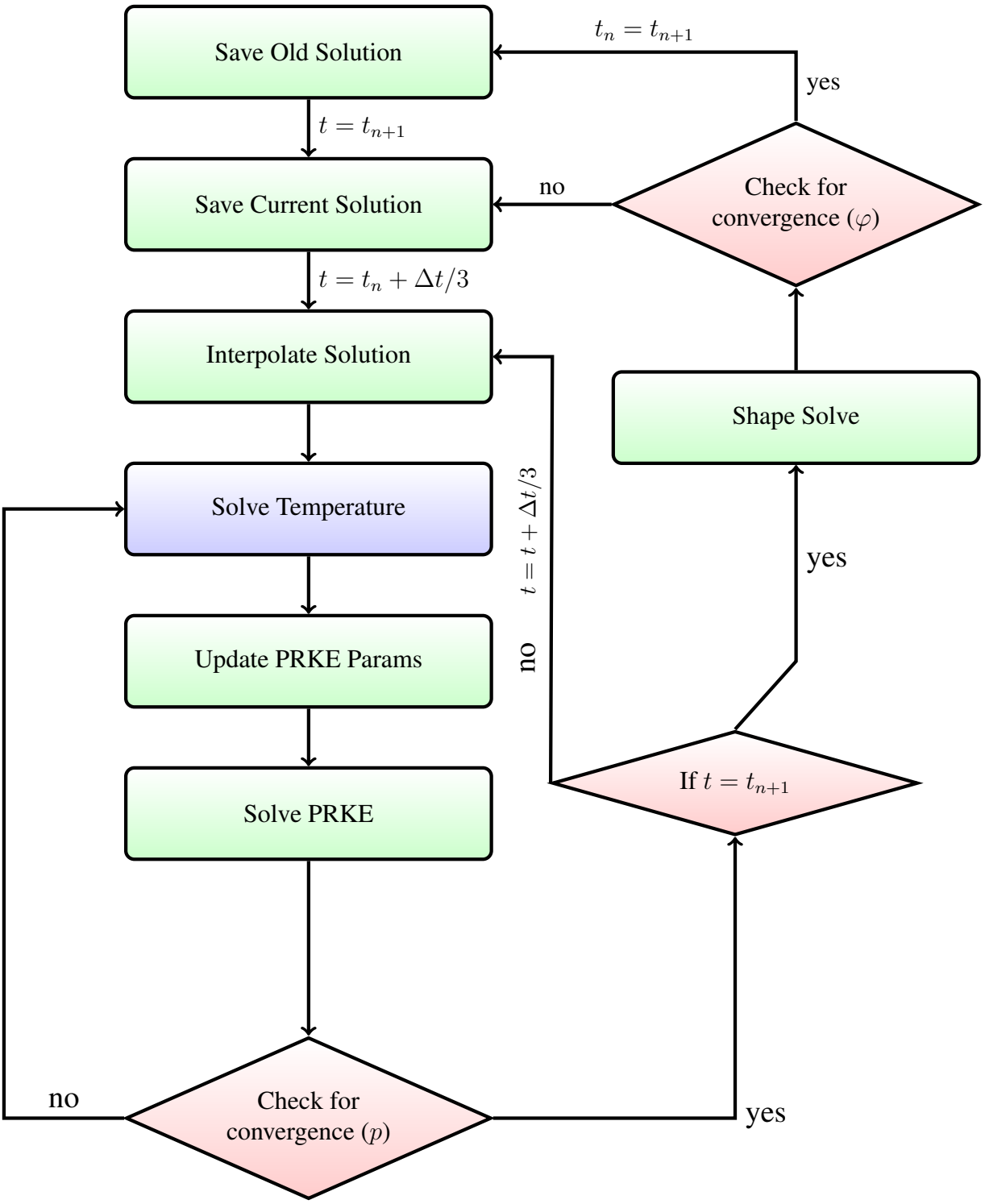

Figure 2.4: Visualization of fixed-point iteration and temperature update process for IQS

2.5.1 Theta Method Time Discretization

A fairly simple way to evaluate the shape equation is to employ the θ-scheme ($0 \leq \theta \leq 1$, explicit when $\theta = 0$, implicit when $\theta = 1$, and Crank-Nicholson when $\theta = 1/2$) [14]. Generally, if there is a function u whose governing equation is $\frac{du}{dt} = f(u,t)$, then the θ-discretization is:

$$\frac{u^{n+1} - u^n}{\Delta t} = (1-\theta)f(u^n, t) + \theta f(u^{n+1}, t)\,. \tag{2.30}$$

Where n is the previous time step and $n+1$ is the time step being evaluated. Applying this to Equation (2.29) yields:

$$\varphi_{n+1} = (IV - \Delta t A_{n+1})^{-1}\left[\Delta t(1-\theta)(A_n\varphi_n + b_n) + \Delta t\theta b_{n+1} + IV\varphi_n\right] \tag{2.31}$$

2.5.2 Backward Difference Formulas

An extension of implicit discretization is the backward difference formulas (BDF) [15]. BDF's can increase the order of error convergence by interpolating solutions from previous time time steps. The general formula for BDF is discribed by Equation (2.32).

$$\varphi_{n+1} = (IV - \Delta t A_{n+1})^{-1}\left[IV\sum_{j=0}^{k-1}\alpha_{jk}\varphi_{n-j} + \Delta t b_{n+1}\right] \tag{2.32}$$

Where k is the order of the error convergence and α_{ij} are coefficients chosen such that the temporal truncation error is minimized. The benifit of using BDF is that any order of convergence can be applied and are all unconditionally stable, so the IQS approximation can easily be validated for high order discretization.

2.5.3 Singly-Diagonally-Implicit Runge-Kutta Method

Singly-Diagonally-Implicit Runge-Kutta Method (SDIRK) is a powerful discretization method that involves solving the linear system in stages to reach a high order solution [16]. Generally, the method can be depicted by using a system where $dy/dt = f(t, y)$ and Equation (2.33).

$$y_{n+1} = y_n + \Delta t \sum_{i=1}^{s} b_i k_i \tag{2.33}$$

Where,

$$k_i = f(t_n + c_i \Delta t, y_n + \Delta t \sum_{j=1}^{i} a_{ij} k_j) \tag{2.34}$$

The coefficients a_{ij}, b_i, and c_i can be represented by a Butcher tableau:

$$\begin{array}{c|cccc} c_1 & a_{11} & & & \\ {}'c_2 & a_{21} & a_{22} & & \\ \vdots & \vdots & \vdots & \ddots & \\ c_s & a_{s1} & a_{s2} & \dots & a_{ss} \\ \hline & b_1 & b_2 & \dots & b_s \end{array}$$

An example used extensively in this research is SDIRK33, which is a third-order method with three stages.

$$\begin{array}{c|ccc} \lambda & \lambda & & \\ \frac{1}{2}(1+\lambda) & \frac{1}{2}(1-\lambda) & \lambda & \\ 1 & \frac{1}{4}(-1+16\lambda-6\lambda^2) & \frac{1}{4}(5-20\lambda+6\lambda^2) & \lambda \\ \hline & \frac{1}{4}(-1+16\lambda-6\lambda^2) & \frac{1}{4}(5-20\lambda+6\lambda^2) & \lambda \end{array}$$

Where $\lambda \approx 0.4358665215$ satisfies $1 - 9\lambda + 18\lambda^2 - 6\lambda^3 = 0$.

2.5.4 Time Adaptation

IQS aims at reducing the time discretization error in the flux solution by splitting the flux into an amplitude (highly resolved at a micro time scale) and a shape (whose time-

dependence is weaker than that of the flux itself). Thus, by construction, the IQS approach may employ larger time-step sizes for comparable temporal error. Further enhancements can be gained by using time adaptation (or time step control) in order to increase or reduce the macro time step size for the shape evaluation, depending on error estimates. A step-doubling technique is chosen as the time adaptation technique [17]. The step doubling technique involves estimating the local error for a certain time step by taking the difference between a solution with one full step ($\varphi^g_{\Delta t}$) and a solution with two half steps ($\varphi^g_{\Delta t/2}$). Note: φ is changed to ϕ for implicit discretization and IQS P-C.

The relative error is computed as follows:

$$e_n = \frac{\left\| \sum_{g=1}^{G} \varphi^g_{\Delta t/2} - \sum_{g=1}^{G} \varphi^g_{\Delta t} \right\|_{L^2}}{\max\left(\left\| \sum_{g=1}^{G} \varphi^g_{\Delta t/2} \right\|_{L^2}, \left\| \sum_{g=1}^{G} \varphi^g_{\Delta t} \right\|_{L^2} \right)} \tag{2.35}$$

If the error is smaller than the user-specified tolerance, e_{tol}, the time step is accepted. In addition, a new time step size is estimated as follows:

$$\Delta t_{new} = S \Delta t \left(\frac{e_{tol}}{e_n} \right)^{\frac{1}{1+q}} \tag{2.36}$$

Where q is the convergence order of the time integration scheme being used and $S \simeq 0.8$ is a safety factor. If the error is larger than the user-specified tolerance, the time step is rejected. A new time step size is estimated using Equation (2.35) as well. This process can be visualized by Figs. 2.5 and 2.6. Where a step involves a full convergence of shape, amplitude, and any multiphysics on the respective time step.

To investigate IQS's performance with step-doubling time adaptation, the adaptation will be applied to implicit discretization method, traditional IQS, and IQS P-C. Each of these methods will be applied to several diffusion problems; the number of time steps taken and the resulting error will be used to compare the methods.

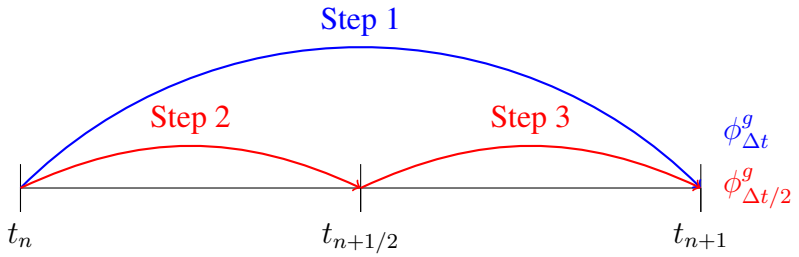

Figure 2.5: Visualization of step doubling process on time-line

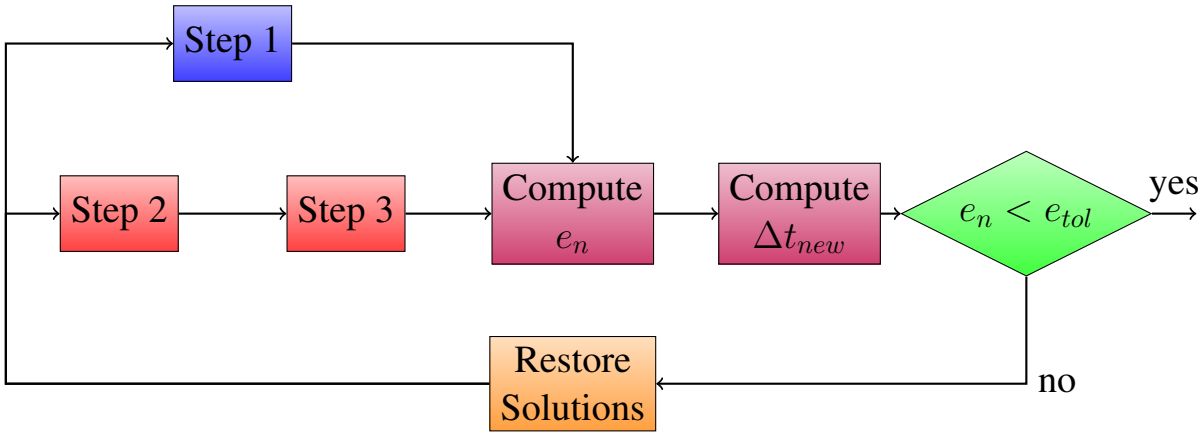

Figure 2.6: Visualization of step doubling process with coding logic

2.6 Delayed Neutron Precursor Updates

This section presents the time-integration method used to solve coupled flux/shape and precursor equations, represented by Equations (1.1a)/(2.1a) and (1.1b)/(2.1b). First, we note that we could keep this system of two time-dependent equations and solve it as a coupled system. However, this is unnecessary and a memory expensive endeavor because the precursor equation is only an ODE and not a PDE. Instead, one may discretize in time the shape equation, which typically requires the knowledge of the precursor concentrations at the end of the time step. This precursor value is taken from the solution, numerical or analytical, of the precursors ODE.

2.6.1 Precursor Evaluation Using Theta Method Time Discretization

A common precursor evaluation technique is using the theta method, described in Section 2.5.1. Applying this to Equation (2.1b):

$$\frac{C^{n+1}-C^{n}}{\Delta t}=(1-\theta)\beta S_f^n p^n-(1-\theta)\lambda C^n+\theta\beta S_f^{n+1}p^{n+1}-\theta\lambda C^{n+1} \tag{2.37}$$

Where S_f is the fission source equivalent for shape ($S_f^n = (\nu\Sigma_f)^n\varphi^n$). Rearranging to solve for the precursor at the end of the time step yields

$$C^{n+1}=\frac{1-(1-\theta)\Delta t\lambda}{1+\theta\Delta t\lambda}C^n+\frac{(1-\theta)\Delta t\beta}{1+\theta\Delta t\lambda}S_f^n p^n+\frac{\theta\Delta t\beta}{1+\theta\Delta t\lambda}S_f^{n+1}p^{n+1} \tag{2.38}$$

Reporting this value of C^{n+1}, one can solve for the shape φ^{n+1} as a function of φ^n and C^n (and p^n, p^{n+1}, $dp/dt|_n$ and $dp/dt|_{n+1}$). Once φ^{n+1} has been determined, C^{n+1} is updated. Applying this technique to implicit discretization is done by changing the definition the fission source ($S_f^n = (\nu\Sigma_f)^n\varphi^n$) and eliminating all p terms.

2.6.2 Analytical Precursor Integration

Another technique to evaluating the precursor equation is to use a exponential operator and integrate the time derivative analytically. Applying this operation to Equation (2.1b) yields:

$$C^{n+1} = C^n e^{-\lambda(t_{n+1}-t_n)} + \int_{t_n}^{t_{n+1}} \beta(t') S_f(t') p(t') e^{-\lambda(t_{n+1}-t')} dt' \tag{2.39}$$

Again, this can be applied to implicit discretization by altering the definition of the fission source and eliminating p. Because S_f is not known continuously over the time step, the integration can be done using any schemet (Riemann, trapezoid, Simpson's, etc.). However, there is a very accurate representation of $p(t)$ over the macro step from the PRKE solve. In order to utilize this information, another possibility is to interpolate S_f linearly over the macro step. Such that:

$$S_f(t) = \frac{t_{n+1}-t}{t_{n+1}-t_n} S_f^n + \frac{t-t_n}{t_{n+1}-t_n} S_f^{n+1} \quad t_n \leq t \leq t_{n+1} \tag{2.40}$$

Applying this to Equation (2.39) yields:

$$C^{n+1} = C^n e^{-\lambda \Delta t} + \left(\hat{a}_2 S_f^{n+1} + \hat{a}_1 S_f^n\right) \beta \tag{2.41}$$

With integration coefficients defined as:

$$\hat{a}_1 = \int_{t_n}^{t_{n+1}} \frac{t_{n+1}-t'}{\Delta t} p(t') e^{-\lambda(t_{n+1}-t')} dt' \tag{2.42}$$

$$\hat{a}_2 = \int_{t_n}^{t_{n+1}} \frac{t'-t_n}{\Delta t} p(t') e^{-\lambda(t_{n+1}-t')} dt' \tag{2.43}$$

The amplitude (p) is included in the integration coefficient because it has been highly accurately calculated in the micro step scheme, so a piecewise interpolation (linear, cubic, etc.) between those points can be done to maximize accuracy.

2.7 Rattlesnake Implementation

Rattlesnake is a MOOSE-based application developed INL specific to solving radiation transport problems with multiphysics capabilities. MOOSE is a finite-element based, multiphysics framework that gives the general architecture for the development of physics application like Rattlesnake. At the heart of Rattlesnake is the action system, which provides a means to consolidate the MOOSE input syntax (which can be quite larger for multigroup transport simulations), so that a user does not have to define every kernel, variable, etc., used in the problem. Rather, the user inputs an equation description (e.g., Diffusion, S_n, P_n, etc.) and a solution method (e.g., SAAF, LS, CFEM, DFEM, etc.), and the action system will incorporate all the necessary physics involved (kernels, boundary conditions, postprocessor, etc.).

2.7.1 Executioner

An IQS excecutioner was created to implement the IQS method. The IQS executioner derives from the Transient executioner in MOOSE. The IQS executioner contains a loop over micro time steps that computes the PRKE solution and then passes p and $\frac{dp}{dt}$ for the Transient executioner to evaluate the shape equation at each macro step. The PRKE solve is performed with a user specified option of backward-Euler, Crank-Nicholson, or SDIRK33. The IQS executioner also supplements Transient Picard iteration process by adding its own error criteria:

$$Error_{IQS} = \left| \frac{\sum_{g=1}^{G} \left(\phi^{*g}, \frac{1}{v^g} \varphi^{g,n} \right)}{\sum_{g=1}^{G} \left(\phi^{*g}, \frac{1}{v^g} \varphi^{g,0} \right)} - 1 \right| \tag{2.44}$$

2.7.2 Action System

The IQS implementation mostly require the specific IQS executioner, described above. However, IQS additional changes are in the Rattlesnake action system in order to support the IQS execution. First, changes needed to be made in order to evaluate the shape equation. The shape equation, after some manipulation, is very similar to the time-dependent governing laws that Rattlesnake already solves. Using multigroup diffusion as an example again, we show the various kernels employed and highlight the new or modified kernels.

$$\frac{\partial}{\partial t}\left(\frac{\varphi^g}{v^g}\right) = \underbrace{\frac{\chi_p^g}{k_{eff}}\sum_{g'=1}^{G}(1-\beta)\nu^{g'}\Sigma_f^{g'}\varphi^{g'}}_{FluxKernel} + \underbrace{\sum_{g'\neq g}^{G}\Sigma_s^{g'\to g}\varphi^{g'}}_{FluxKernel} - \underbrace{\left(-\nabla\cdot D^g\nabla\right)\varphi^g}_{FluxKernel} - \underbrace{\Sigma_r^g\varphi^g}_{FluxKernel}$$
$$\underbrace{-\frac{1}{v^g}\boxed{\overbrace{\frac{1}{p}\frac{dp}{dt}}^{FromExecutioner}}\varphi^g}_{IQSKernel} + \underbrace{\frac{1}{p}\sum_{i=1}^{I}\chi_{d,i}^g\lambda_i C_i}_{ModifiedFluxKernel} \tag{2.45}$$

To enable Rattlesnake to solve this equation, an IQS removal kernel was created to evaluate $\sum_{g=1}^{G}\frac{1}{v^g}\frac{1}{p}\frac{dp}{dt}\varphi^g$ and added when the IQS executioner is called. Also, the precursor kernel was modified to include the $\frac{1}{p}$ term. Finally, the precursor auxkernel that evaluates Equation (2.1b) using the analytical integration method described in Section 2.6.

2.7.3 PRKE coefficients

In order to evaluate the PRKE coefficients, defined by Equations 2.3a - 2.3c, four postprocessors were created. The parameter calculations were separated by $\frac{\bar{\beta}_i}{\Lambda}$ numerator, $\bar{\lambda}_i$ numerator/denominator, $\frac{\rho-\bar{\beta}}{\Lambda}/\frac{\bar{\beta}}{\Lambda}$ denominator, and $\frac{\rho-\bar{\beta}}{\Lambda}$ numerator. The first three are relatively simple, only relying on material properties and solution quantities, then computing the elemental integral. The $\frac{\rho-\bar{\beta}}{\Lambda}$ numerator requires the use of the MOOSE `save_in`

feature. This feature saves the residual from a calculated kernel or boundary contribution in the shape evaluation to an auxiliary variable. The postprocessor then computes the inner product of this variable and the initial adjoint solution. After each of these postprocessors are evaluated, a user object pulls together all the values and performs the numerator/denominator divisions. The resulting values are then passed to the executioner for the PRKE solve.

2.7.4 Other Action Systems

For simplicity, IQS implementation has only been described for CFEM diffusion. However, Rattlesnake has other action systems capable of transient simulation, where IQS can be implemented and be effective. One of these action systems is DFEM diffusion, where the only major difference from CFEM is the diffusion term in Equations (1.1a) and (2.1a). However, in the derivation for IQS, this term is unaffected between shape and flux evaluation. So saving the residual for this diffusion kernel in the `save_in` variable is the only alteration to this action for IQS to function.

Additional action systems involve transport, but it is evident from Section 2.1.1 that IQS implementation in these is straightforward as well. The main differences between a diffusion implementation and a transport implementation are outlined below:

1. The form of the operators in the shape equations is different, but Rattlesnake has already implemented all the kernels necessary to represent these operators. So no change is necessary to these kernels is necessary for IQS. Additionally, the $\frac{1}{v^g}\frac{1}{p}\frac{dp}{dt}$ is the same, so both action systems can use the same kernel.

2. The PRKE parameters also change because of the operators. For the $(\rho - \bar{\beta})$ parameter, the same post-processor can be used with the `save_in` functionality in MOOSE. The post-processor for $\bar{\beta}_i$ must be re-written for transport, but takes a very similar form as diffusion.

IQS will be made available to any action system capable of transient simulation, which includes:

- CFEM-Diffusion
- DFEM-Diffusion
- SAAF-CFEM-SN
- SAAF-CFEM-PN
- LS-CFEM-SN
- DFEM-SN

2.7.5 Predictor-Corrector Modification

In order to preserve the already implemented standard version of IQS, an option in the IQS executioner was created to specify which method is desired. Because the diffusion solve is flux instead of shape, when predictor-corrector option is specified, the IQS removal kernel ($\frac{1}{v^g}\frac{1}{p}\frac{dp}{dt}$) and the modified precursor kernel are bypassed, while all the post-processors are still executed. However, it is difficult to rescale the flux to shape before the PRKE parameter postprocessor are executed. So the parameters are computed using the full flux, but amplitude is space independent and comes out of the integrals. As seen in parameter definitions, when shape is replaced with flux, the amplitude comes out of the integral and cancels out. So the conversion of the predicted flux in Equation (2.20) to shape is unnecessary if the corrected flux is solved with Equation (2.46). After obtaining the corrected flux, the precursors are re-evaluated using a `EXEC_LINEAR` statement.

$$\underbrace{\phi^g_{n+1}}_{\text{corrected}} = \underbrace{\phi^g_{n+1}}_{\text{predicted}} \frac{K_0}{K_{n+1}} p_{n+1} \tag{2.46}$$

2.7.6 Input

The input file for IQS is very similar to the current transient diffusion input file. The IQS input has a different executioner type and parameters. The executioner type is simply IQS and input parameters include the number of micro time steps per macro step, the IQS error tolerance, and the initial power. The Rattlesnake transient action system currently requires a multi-app and transfer to compute and pass the initial ϕ and k_{eff}, which is present in the transient input deck. However, IQS also requires an initial evaluation of the adjoint flux, for the weighting function. So another input file and multi-app transfer was made for the adjoint calculation.

Below is the syntax for the executioner block for an IQS input file. The `predictor_corrector` logical determines whether to do IQS P-C or regular IQS. The `IQS_error_tol` is the tolerance for the IQS error represented by Equation (2.44) and will at most `picard_max_its` iterations until convergence. The `prke_scheme` defines the time discretization used for the PRKE solution. Where `RK` is SDIRK33, `CN` is Crank-Nicholson, and `IE` is implicit-Euler.

```
[Executioner]
  type = IQS
  predictor_corrector = true/false
  picard_max_its = 5
  ...
  n_micro = 10000
  IQS_error_tol = 1e-7
  prke_scheme = 'RK'
[]
```

Since IQS needs to use the adjoint solution for the PRKE parameter evaluation, auxiliary variables need to be created for each group in the input file. Below is an example of their definition:

```
[AuxVariables]
  [./adjoint_flux_g0]
    family = LAGRANGE
    order = FIRST
  [../]
```

```
  [./adjoint_flux_g1]
    family = LAGRANGE
    order = FIRST
  [../]
  ...
[]
```

Below is the syntax for the multi-app block to perform forward and adjoint steady-state evaluations:

```
[MultiApps]
 [./initial_solve]
   type = FullSolveMultiApp
   execute_on = initial
   input_files = initial.i
 [../]
 [./adjoint_solve]
   type = FullSolveMultiApp
   execute_on = initial
   input_files = adjoint.i
 [../]
[]
```

Below is the syntax for the Transfer block to copy the initial and adjoint solutions from the multi-apps.

```
[Transfers]
 [./copy_solution]
   type = TransportSystemVariableTransfer
   direction = from_multiapp
   multi_app = initial_solve
   execute_on = initial
   from_transport_system = diff
   to_transport_system = diff
 [../]
 [./copy_adjoint]
   type = MultiAppVariableTransfer
   execute_on = initial
   direction = from_multiapp
   multi_app = adjoint_solve
   from_variables = 'sflux_g0 sflux_g1 ...'
   to_variables = 'adjoint_flux_g0 adjoint_flux_g1 ...'
 [../]
 [./copy_eigenvalue]
   type = EigenvalueTransfer
   execute_on = initial
   direction = from_multiapp
   multi_app = initial_solve
 [../]
[]
```

3. KINETICS EXAMPLES

Neutron dynamics is the study of the time-dependent nature of neutrons in a reactor. More specifically, there is no coupling of neutron behavior with other physics, like thermal hydraulic feedback. This section describes kinetics examples that IQS is tested with and analysis of its performance. The examples range in complexity and application. The first is a one-dimensional problem, designed for the prototype code in MATLAB. The next four are from the Argonne National Lab (ANL) Benchmark Problem Book (BPB), and are common problems for testing codes and developing methods [13].

3.1 One Dimensional Prototype Problem

This example is very simple and computes quickly; it entails a one dimensional, homogeneous 400 cm slab with a heterogenous perturbation in absorption cross section. Figure 3.1 shows how the regions of the slab are divided and Table 3.1 shows the initial material properties. Regions 2, 3, and 4 have slope perturbations at different points in time, Table 3.2 shows the values of the absorption cross-section in each region at the times of interest. The values of Σ_a between these times of interest are linear interpolations between the given values.

1	1	1	1	2	3	1	1	1	1	1	1	1	1	4	4	1	1	1	1

Figure 3.1: 1-D slab region identification

Figure 3.2 shows the resulting baseline relative power profile of the one-dimensional

Table 3.1: 1-D slab material properties and problem parameters

$D(cm)$	$\Sigma_a(cm^{-1})$	$\nu\Sigma_f(cm^{-1})$	$v(cm/s)$	β	$\lambda(s^{-1})$
1.0	1.1	1.1	1,000	0.006	0.1

Table 3.2: 1-D slab absorption cross-section at times of interest

Region	Material Property	0.0 s	0.1 s	0.6 s	1.0 s	1.7 s
2	$\Sigma_a(cm^{-1})$	1.1	1.1	1.095	1.095	1.095
3	$\Sigma_a(cm^{-1})$	1.1	1.1	1.09	1.09	1.1
4	$\Sigma_a(cm^{-1})$	1.1	1.1	1.105	1.105	1.105

problem. The baseline was computed using MATLAB's ode15s function which is a embedded Runge-Kutta time adaptive method for stiff problems, the error tolerance was set very tightly (10^{-12}). This baseline computation is used to compute the error of the other time discretization methods. Figure 3.3 shows the shape profile at various times during the transient. It is apparent that the shape is very time-dependent, so it is expected that IQS has marginal accuracy gain for a given time step.

3.1.1 IQS Iteration Convergence

3.1.2 Time Step Convergence

In order to evaluate the performance and error convergence of IQS, the slab was simulated with varying time discretization methods and time step sizes. Figure **??** shows these convergence plots of five different discretization methods for implicit discretization, IQS, and IQS P-C. These plots were generated from the results using the MATLAB prototype program. The plots show that IQS and IQS P-C are convergent through fourth order BDF. Third order SDIRK did not show third order convergence, but, through extensive testing, SDIRK shows non-convergent behavior for too stiff of problems.

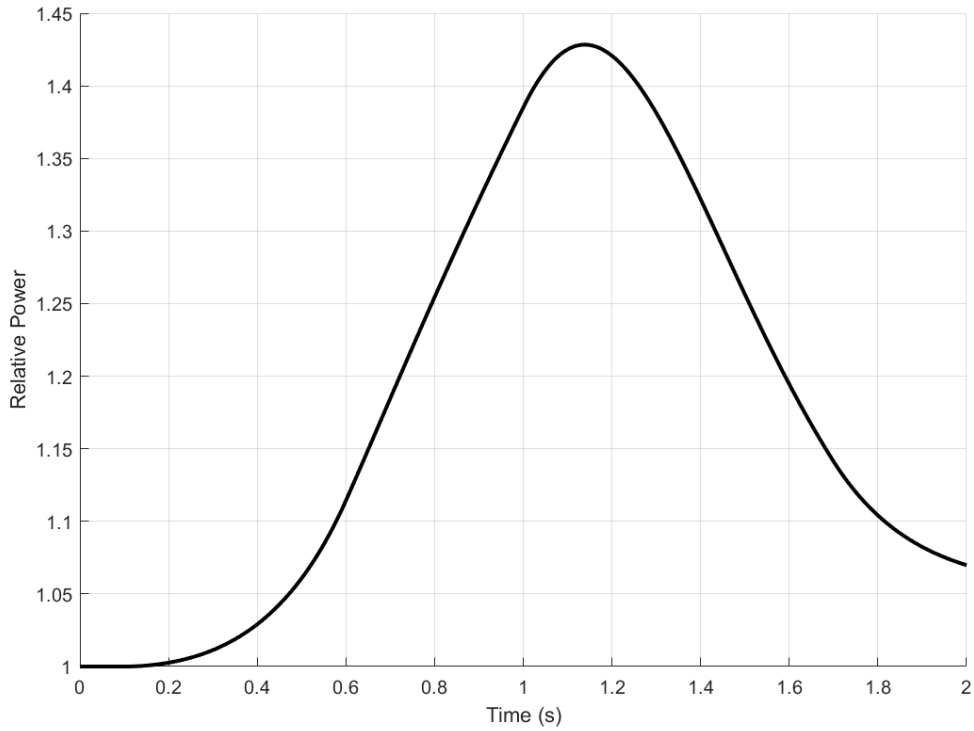

Figure 3.2: Baseline power profile of 1D slab

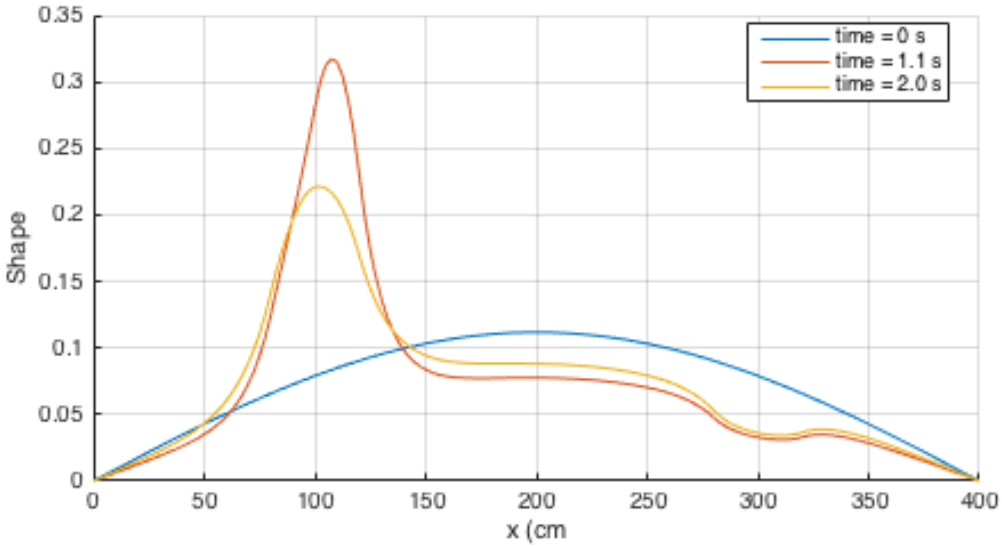

Figure 3.3: Flux profile of 1D slab at various times

There are higher discretization order that can be tested, but most practical application do not go beyond second order. This paper shows an analysis of the first publicized application of IQS with higher than second order discretization, which exposed unforeseen properties of IQS. When using higher order techniques, the interpolation of PRKE parameters and shape for precursor integration become important to consider. Every other application that was investigated linearly interpolates parameters for the PRKE evaluation. Similarly, the shape used for the integration of the ODE for the precursors needs to have higher order interpolation to preserve high order error convergence. This interpolation was done using Lagragian and Hermite methods, both leading to successful convergence.

The 1D slab problem was also applied to the Rattlesnake implementation of IQS. Figure 3.5 shows the error convergence for implicit Euler and BDF2 discretization of the three methods. The results differ slightly from the prototype, especially in the fact that IQS P-C performs better than IQS. Since Rattlesnake uses a PJFNK solver for the FEM model, number of time steps isn't strictly proportional to the execution time. Figure 3.6 shows the error of the three methods as compared to the number of linear GMRES iterations, which is a better mark for comparison in computation time. This figure shows that IQS performs worse than implicit discretization for most time-step sizes, but IQS P-C performs significantly better. This is due to the fact that IQS needs to iterate between amplitude and shape to resolve its nonlinearity.

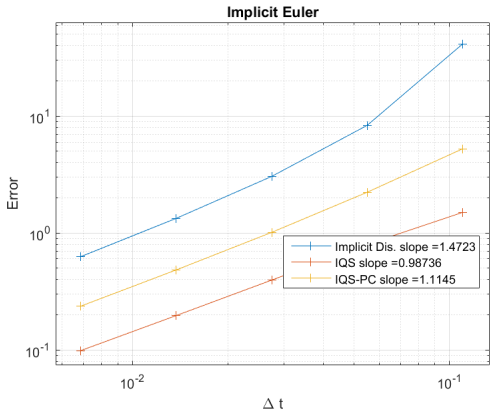

(a) Implicit Euler

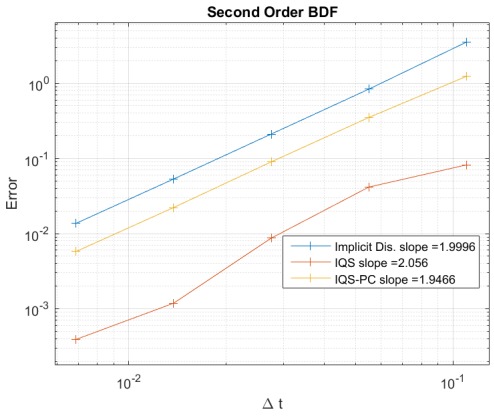

(b) BDF2

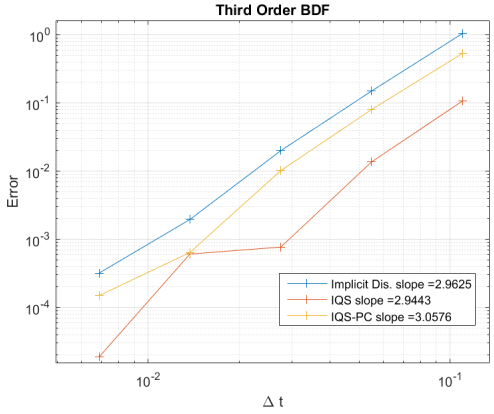

(c) BDF3

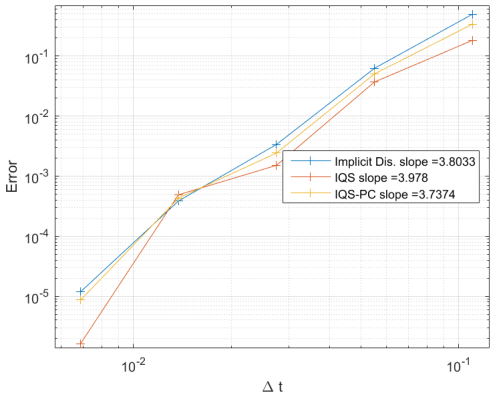

(d) BDF4

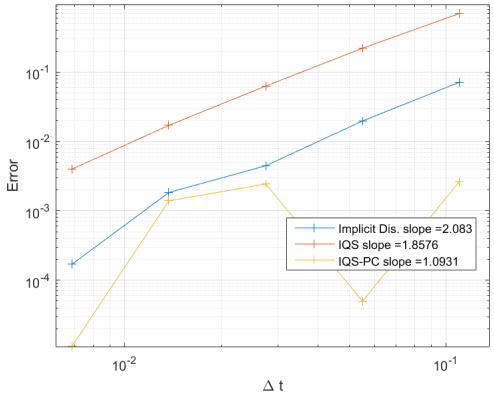

(e) SDIRK33

Figure 3.4: Error convergence plots of implicit discretization, IQS, and IQS P-C with various time discretization schemes

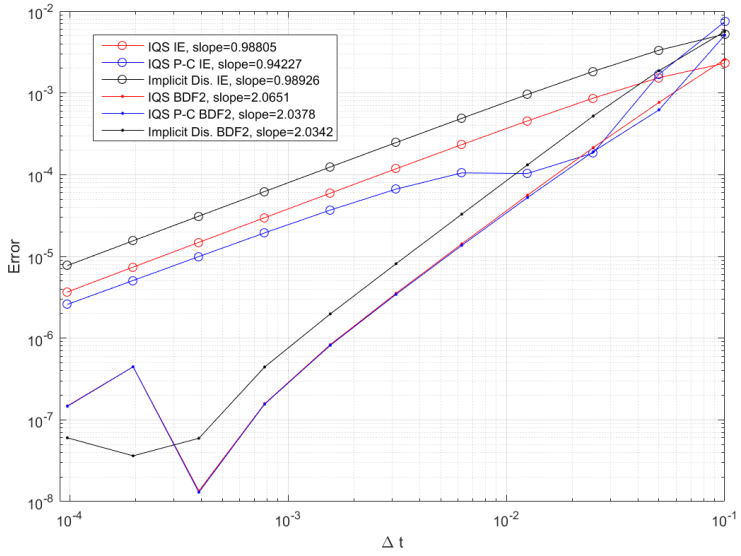

Figure 3.5: Error convergence plots of implicit discretization, IQS, and IQS P-C from Rattlesnake implementation

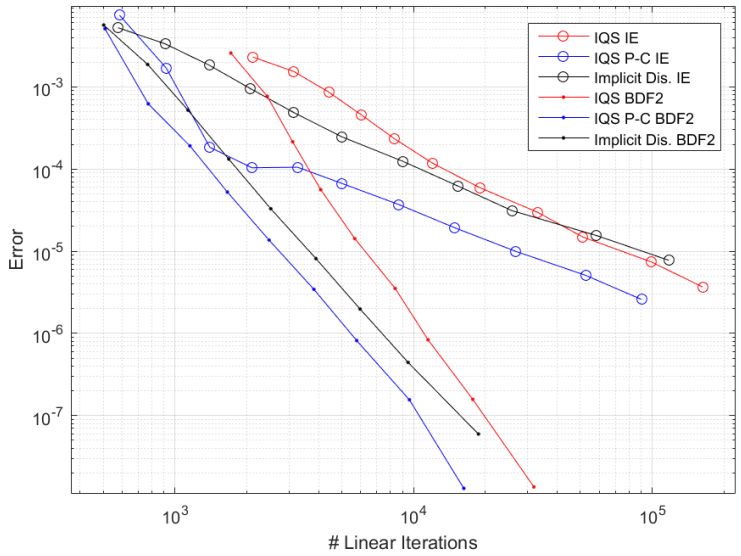

Figure 3.6: Error convergence plots of implicit discretization, IQS, and IQS P-C vs. number of GMRES iterations

3.2 TWIGL Benchmark

This benchmark problem originates from the Argonne National Lab Benchmark Problem Book [13]. It is a 2D, 2-group reactor core model with no reflector region shown in Figure 3.7 [18]. This example is meant to be of progressive complexity from the previous example. The transient of this reactor is very geometrically symmetrical with very little temporal shape change. Therefore, IQS is expected to perform significantly better than the implicit discretization method. Table 3.3 shows the material properties of each fuel region and the ramp perturbation of Material 1.

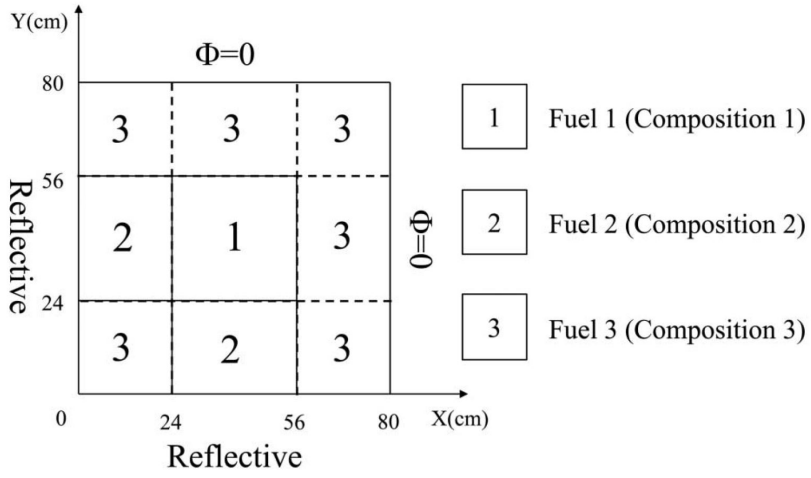

Figure 3.7: TWIGL benchmark problem description

3.2.1 TWIGL Convergence Analysis

Figs. 3.8 and 3.9 show the IQS solution as compared with the implicit discretization solution. It is important to note the IQS shape plot is scaled differently than the Brute Force flux plot (Figure 3.9) because the amplitude term is not included, but the gradients

Table 3.3: TWIGL benchmark material properties and slope perturbation

Material	Group	$D(cm)$	$\Sigma_a(cm^{-1})$	$\nu\Sigma_f(cm^{-1})$	χ	$\Sigma_s(cm^{-1})$ $g \to 1$	$\Sigma_s(cm^{-1})$ $g \to 2$
1	1	1.4	0.010	0.007	1.0	0.0	0.01
	2	0.4	0.150	0.200	0.0	0.0	0.00
2	1	1.4	0.010	0.007	1.0	0.0	0.01
	2	0.4	0.150	0.200	0.0	0.0	0.00
3	1	1.3	0.008	0.003	1.0	0.0	0.01
	2	0.5	0.050	0.060	0.0	0.0	0.00
	ν	$v_1(cm/s)$	$v_2(cm/s)$	β	$\lambda(1/s)$		
	2.43	1.0E7	2.0E5	0.0075	0.08		

Material 1 ramp perturbation:

$\Sigma_{a,2}(t) = \Sigma_{a,2}(0) \times (1 - 0.11667t) \quad t \leq 0.2s$

$\Sigma_{a,2}(t) = \Sigma_{a,2}(0) \times (0.97666t) \quad t > 0.2s$

of colors is comparable. These plots show that IQS is consistent in more complex, higher dimensional problems in Rattlesnake. These plots also serve to illustrate that IQS has a much more accurate solution, even at a significantly larger time step than the implicit discretization. In order to demonstrate asymptotic convergence of IQS, implicit Euler (IE) and second order BDF (BDF2) were applied to the TWIGL simulation. Figure 3.10 plots the error convergence of IQS and the implicit discretization methods. The curves show the impressive convergence of IQS for the highly transient TWIGL example. The slope indicated in the legend are the linear slope of curves on the log plot, these slopes should be similar to the order of the method (1 for IE and 2 for BDF2). IQS shows a increased order because the PRKE is performing much of accuracy convergence and it is computed using SDIRK33, a third order method.

3.2.2 TWIGL with Step Doubling Time Adaptation

Table 3.4 and Figure 3.11 show the results for TWIGL with time adaptation. The results show that both IQS methods perform exceptionally well compared to implicit dis-

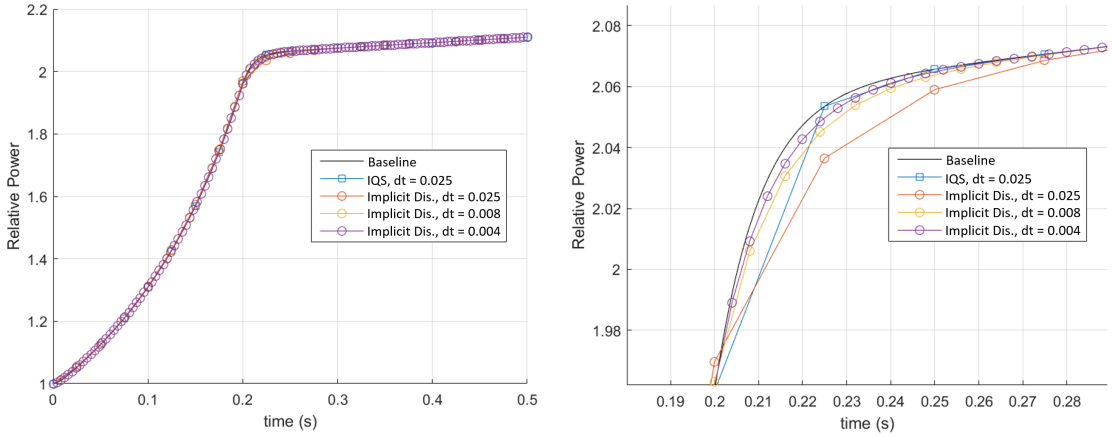

(a) Power profile for entire transient

(b) Power at cusp of profile

Figure 3.8: Power level comparison of TWIGL Benchmark

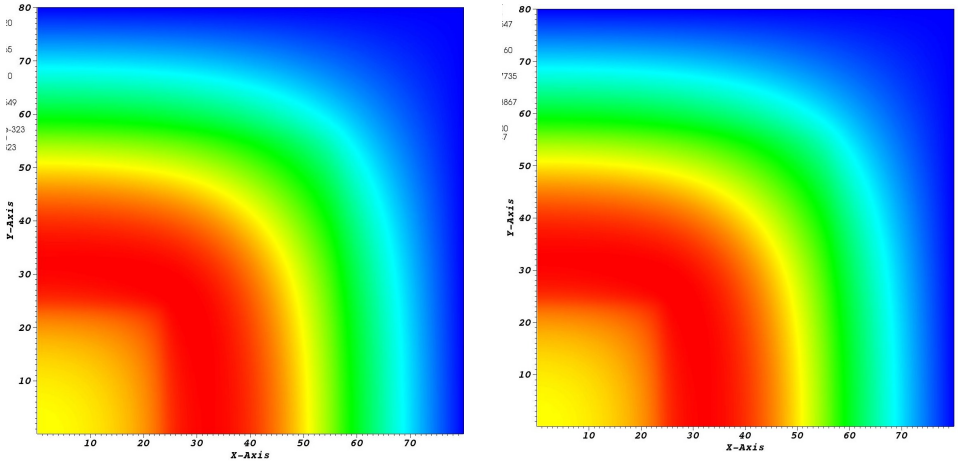

(a) Implicit Discretization flux

(b) IQS Shape

Figure 3.9: TWIGL Benchmark flux/shape comparison at $t = 0.2$

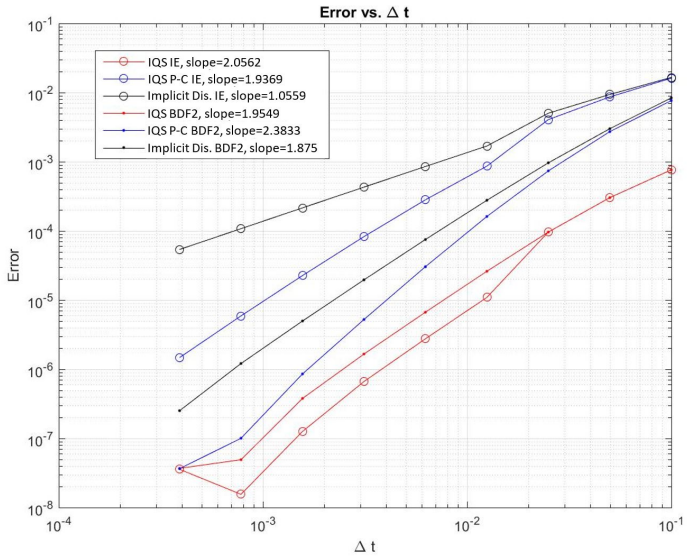

Figure 3.10: Error convergence comparison of TWIGL Benchmark

cretization. It also shows that traditional IQS performed better with large e_{tol}, while IQS P-C was better with smaller e_{tol}.

Table 3.4: TWIGL step doubling results

		Implicit Discretization			IQS			IQS P-C		
Test	e_{tol}	Error	Steps	Solves	Error	Steps	Solves	Error	Steps	Solves
1	0.05	0.00012677	9	29	0.03380433	4	20	0.00323100	4	9
2	0.01	3.5555e-05	11	35	0.00166991	5	40	0.00263068	5	12
3	0.005	4.0364e-05	11	31	0.00886584	5	40	0.00160486	6	21
4	0.001	0.00294822	33	122	0.02976305	5	36	1.7527e-05	10	35
5	0.0005	0.00099778	39	131	0.00143781	6	55	1.4185e-05	16	74
6	0.0001	0.00019510	78	236	0.00016175	8	65	6.2903e-06	19	78
7	5.0e-05	0.00018372	112	342	6.0328e-05	12	163	1.5247e-06	24	92
8	1.0e-05	8.0564e-05	263	794	7.7103e-05	379	5729	9.8321e-07	48	210

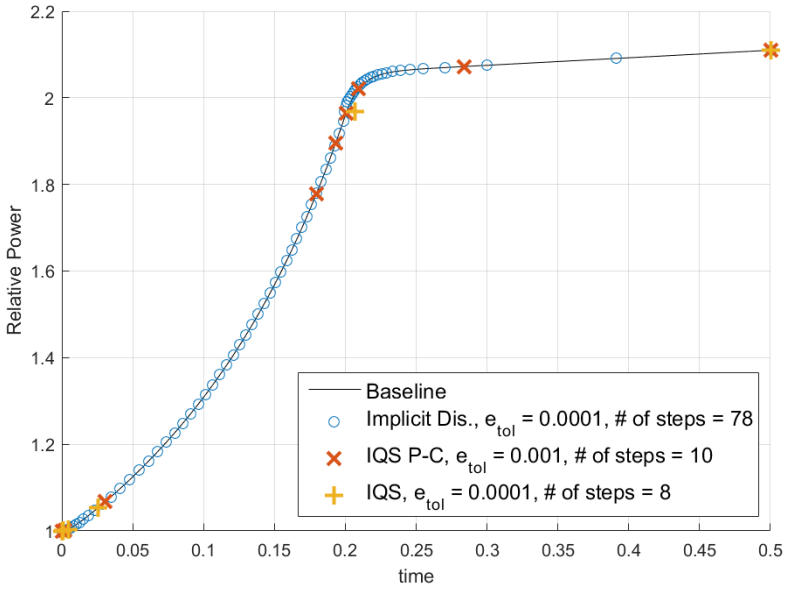

Figure 3.11: Power level comparison of TWIGL Benchmark with time adaptation

3.3 C5G7-TD Benchmark

The C5G7 benchmark is a MOX fueled, pressurized water reactor (PWR) minicore configuration. The C5G7 geometry depicted in Fig. 3.12 comprises a 2-by-2 array of UO_2 and MOX assemblies surrounded by moderator. In Fig. 3.12 vacuum and reflective boundary conditions are denoted by V and R, respectively. The fuel pins are not homogenized, each pin cell is comprised of a fuel pin, fission chamber, or guide tube surrounded by moderator as depicted in Fig. 3.13. The cladding and gap are homogenized into the fuel and are not explicitly modeled. Each assembly is made up of a regular 17-by-17 grid of pin cells. Seven energy-group cross sections for the seven material regions are given in [**?**]. The energy group boundaries are provided in Table 3.5; three of the seven energy groups are fast, four are thermal.

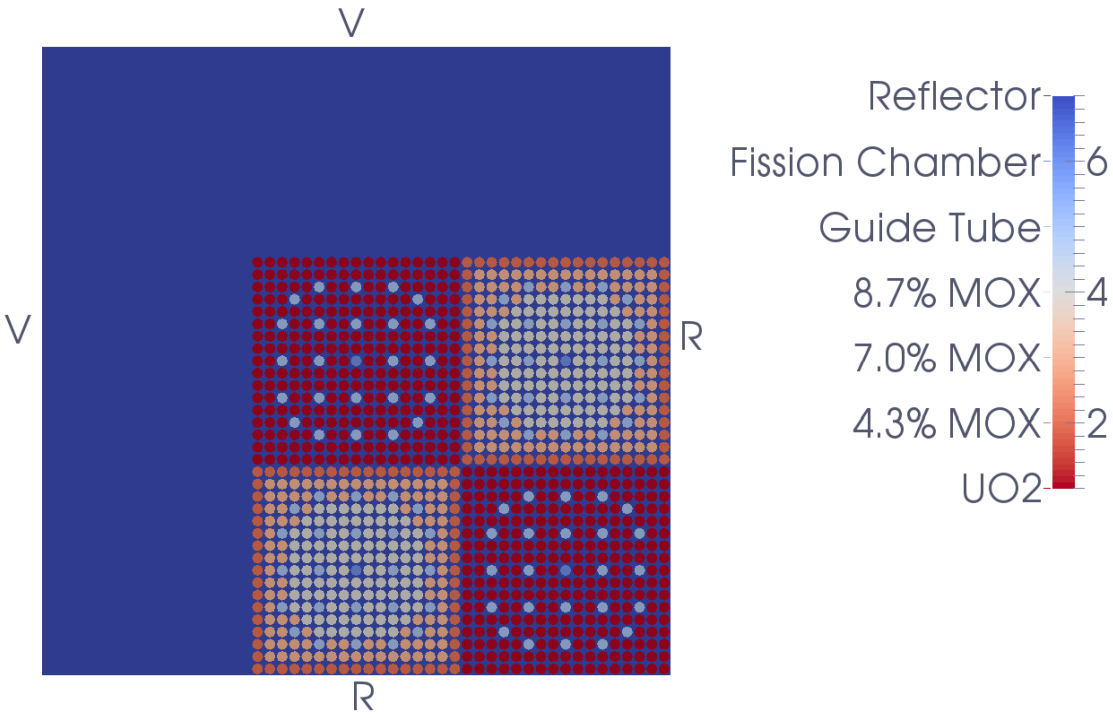

Figure 3.12: Geometry of the two-dimensional C5G7 benchmark problem. Boundary conditions are vacuum (V) or reflective (R).

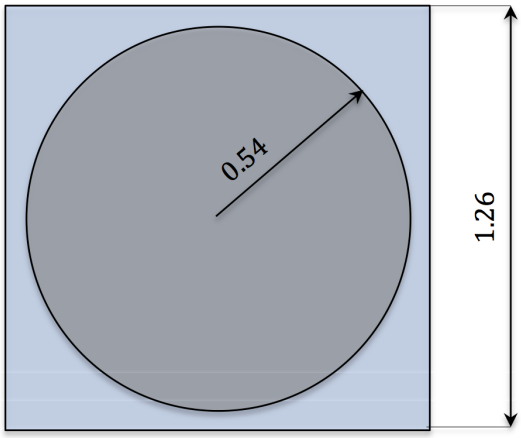

Figure 3.13: Geometry of a C5G7 pin-cell.

Table 3.5: Energy group boundaries for C5G7 MOX benchmark.

Group	Upper Energy
1	20 MeV
2	1 MeV
3	500 keV
4	3 eV
5	0.625 MeV
6	0.1 MeV
71	0.02 MeV

3.4 LMW Benchmark?

4. DYNAMICS EXAMPLES

Reactor dynamics is the study of the time-dependent behavior of reactors as an entire system. This study includes the physical nature of neutrons and their feedback with power generation. This feedback includes coupling with other physical properties such as temperature, fluids, material dynamics, etc. This section describes several dynamics examples, including the LRA benchmark and two TREAT experiments. These examples are of increased complexity from the kinetics examples of Section **??**. This section also analyzes IQS's performance with these, which is vital for verification of IQS in real-world problems.

4.1 LRA Benchmark

The LRA benchmark is a two-dimensional, two-group neutron diffusion problem with adiabatic heat-up and Doppler feedback in thermal reactor [13]. It is a super prompt-critical transient. To have better understanding on the cross sections given later, we present

the equations here:

$$-\frac{1}{v_1}\frac{\partial \phi_1}{\partial t} = -\nabla\cdot D_1\nabla\phi_1 + (\Sigma_{a,1}+\Sigma_{s,1\to 2})\phi_1 - \nu(1-\beta)S_f - \sum_{i=1}^{2}\lambda_i C_i, \tag{4.1a}$$

$$-\frac{1}{v_2}\frac{\partial \phi_2}{\partial t} = -\nabla\cdot D_2\nabla\phi_1 + \Sigma_{a,2}\phi_2 - \Sigma_{s,1\to 2}\phi_1, \tag{4.1b}$$

$$S_f = \sum_{g=1}^{2}\Sigma_{f,g}\phi_g, \tag{4.1c}$$

$$\frac{\partial C_i}{\partial t} = \nu\beta_i f - \lambda_i C_i, \quad i = 1,2, \tag{4.1d}$$

$$\frac{\partial T}{\partial t} = \alpha f, \tag{4.1e}$$

$$\Sigma_{a,1} = \Sigma_{a,1}(\vec{r}, t=0)\left[1+\gamma\left(\sqrt{T}-\sqrt{T_0}\right)\right], \tag{4.1f}$$

$$P = \kappa S_f, \tag{4.1g}$$

where ϕ_1, ϕ_2 are the fast and thermal fluxes; v_1, v_2 are the averaged neutron velocities; $\Sigma_{a,1}, \Sigma_{a,2}$ are the absorption cross sections; $\Sigma_{s,1\to 2}$ is the fast-to-thermal scattering cross section; $\Sigma_{f,1}, \Sigma_{f,2}$ are the fission cross sections; ν is the averaged number of neutrons emitted per fission; β_1, β_2 are the delayed neutron precursor fractions and $\beta = \beta_1 + \beta_2$; C_1, C_2 are the delayed neutron precursor concentrations; λ_1, λ_2 are the decay constants of the delayed neutron precursors; S_f is the fission reaction rate; P is the power density; T is the temperature; κ is the averaged power released per fission; α is the combination of κ and the specific heat capacity; γ is the Doppler feedback coefficient; $T_0 = T(\vec{r}, t=0)$. The two-group diffusion equation are solved with zero flux boundary conditions on external surfaces, reflecting conditions at symmetry boundaries and steady state initial conditions

which are obtained by solving

$$-\nabla\cdot D_1\nabla\phi_1 + (\Sigma_{a,1} + \Sigma_{s,1\to 2})\phi_1 = \frac{1}{k}\sum_{g=1}^{2}\nu\Sigma_{f,g}\phi_g, \tag{4.2}$$

$$-\nabla\cdot D_2\nabla\phi_1 + \Sigma_{a,2}\phi_2 = \Sigma_{s,1\to 2}\phi_1. \tag{4.3}$$

The eigenvalue k is used to modify the fission cross section for the transient simulations with $\frac{1}{k}\Sigma_{f,g}, g = 1, 2$. The initial flux distribution shall be normalized such that the averaged power density

$$\bar{P} \equiv \frac{\int_{V_{core}} P(\vec{r}, t=0)d\vec{r}}{\int_{V_{core}} d\vec{r}}, \tag{4.4}$$

where V_{core} is the core region with fuels, is equal to $10^{-6}W\cdot cm^{-3}$. The initial precursor concentrations are in equilibrium with the initial critical flux distribution.

The geometry is illustrated in Figure 4.1.

Initial two-group constants are presented in Table 4.1. ν is equal to 2.43. Axial bulking $B^2 = 10^{-4}$ is applied for both energy groups. Delayed neutron data are presented in Table 4.2. All fuel materials have the same delayed neutron data. Some scalar data are listed in Table 4.3.

The transient is initiated by changing the thermal absorption cross section as the following:

$$\Sigma_{a,2}(t) = \Sigma_{a,2}(t=0)\begin{cases} 1 - 0.0606184t, & t \le 2 \\ 0.8787631, & t > 2 \end{cases} \tag{4.5}$$

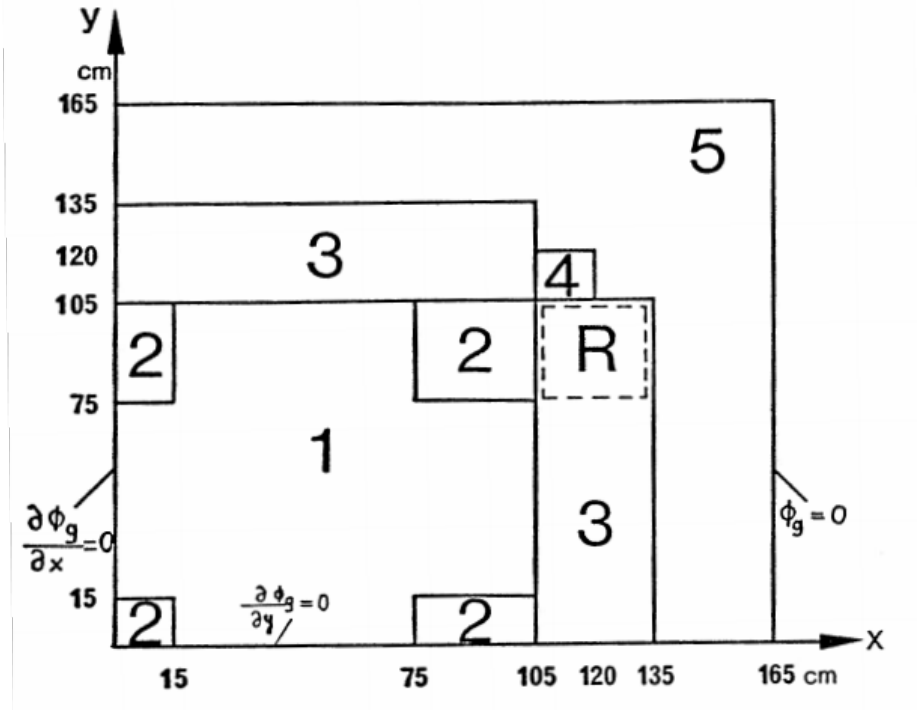

Figure 4.1: LRA benchmark geometry with region assignment.

Table 4.1: LRA benchmark initial two-group constants.

Region	Material	Group g	D_g (cm)	$\Sigma_{a,g}$ (cm^{-1})	$\nu\Sigma_{f,g}$ (cm^{-1})	$\Sigma_{s,1\to2}$ (cm^{-1})	χ_g	v_g $(cm \cdot s^{-1})$
1	Fuel 1 with rod	1	1.255	0.008252	0.004602		1	3.0×10^7
		2	0.211	0.1003	0.1091	0.02533	0	3.0×10^5
2	Fuel 1 without rod	1	1.268	0.007181	0.004609		1	3.0×10^7
		2	0.1902	0.07047	0.08675	0.02767	0	3.0×10^5
3	Fuel 2 with rod	1	1.259	0.008002	0.004663		1	3.0×10^7
		2	0.2091	0.08344	0.1021	0.02617	0	3.0×10^5
4	Fuel 2 without rod	1	1.259	0.008002	0.004663		1	3.0×10^7
		2	0.2091	0.073324	0.1021	0.02617	0	3.0×10^5
5	Reflector	1	1.257	0.0006034	-		-	3.0×10^7
		2	0.1592	0.01911	-	0.04754	-	3.0×10^5

Table 4.2: LRA benchmark delayed neutron data.

Group i	β_i	λ_i (s^{-1})	$\chi_{d,i,1}$	$\chi_{d,i,2}$
1	0.0054	0.0654	1	0
2	0.001087	1.35	1	0

Table 4.3: LRA benchmark scalar values.

Meaning	Notation	value
Axial buckling for both energy groups	B_g^2	10^{-4} (cm^{-2})
Mean number of neutrons per fission	ν	2.43
Conversion factor	α	3.83×10^{-11} $(K \cdot cm^3)$
Feedback constant	γ	3.034×10^{-3} $(K^{1/2})$
Energy released per fission	κ	3.204×10^{-11} $(J/fission)$
Initial and reference temperature	T_0	300 (K)
Active core volume	V_{core}	17550 (cm^2)

where t is time in seconds.

4.2 TREAT Transient-15 Problem

4.3 TREAT M8-CAL Problem

REFERENCES

[1] D. Gaston, C. Newman, G. Hansen, , and D. Lebrun-Grandie, "Moose: A parallel computational framework for coupled systems of nonlinear equations," *Nucl. Engrg. Design*, vol. 239, pp. 1768 – 1778, 2009.

[2] Y. Wang, "Nonlinear diffusion acceleration for multigroup transport equation discretized with sn and continuous fem with rattlesnake," in *Proc. International Conference on Mathematics and Computational Methods Applied to Nuclear Science & Engineering, Idaho*, 2013.

[3] J. J. Duderstadt and L. J. Hamilton, *Nuclear reactor analysis*. Wiley, 1976.

[4] K. Ott, "Quasi-static treatment of spatial phenomena in reactor dynamics," *Nuclear Science and Engineering*, vol. 26, p. 563, 1966.

[5] S. Dulla, E. H. Mund, and P. Ravetto, "The quasi-static method revisited," *Progress in Nuclear Energy*, vol. 50, no. 8, pp. 908 – 920, 2008.

[6] M. Sissnoui, J. Koclas, and A. Hébert, "Solution of the improved and generalized quasistatic methods by kaps and rentrop integration scheme with stepsize control," *Annals of Nuclear Energy*, vol. 22, pp. 763–774, 1995.

[7] J. Koclas, M. Sissnoui, and A. Hébert, "Solution of the improved and generalized quasistatic methods by kaps and rentrop integration scheme with stepsize control," *Annals of Nuclear Energy*, vol. 23, pp. 901–907, 1996.

[8] J. Devooght, B. Arien, E. H. Mund, and A. Siebertz, "Fast reactor transient analysis using the generalized quasi-static approximation," *Nuclear Science and Engineering*, vol. 88, pp. 191–199, 1984.

[9] A. Monier, *Application of the Collocation Technique to the Spatial Discretization of the Generalized Quasistatic Method for Nuclear Reactors*. PhD thesis, Université de Montréal, 1991.

[10] D. E. K. D. A. Knoll, "Jacobian-free newton-krylov methods: a survey of approaches and applications," *Journal fo Computational Physics*, vol. 193, pp. 357–397, 2004.

[11] H. IKEDA and T. TAKEDA, "Development and verification of an efficient spatial neutron kinetics method for reactivity-initiated event analyses," *Journal of Nuclear Science and Technology*, vol. 38, pp. 496–515, 2001.

[12] S. Goluoglu and H. L. Dodds, "A time-dependent, three-dimensional neutron transport methodology," *Nuclear Science and Engineering*, vol. 139, pp. 248–261, 2001.

[13] Argonne Code Center, "Benchmark problem book, anl- 7416, suppl. 2," tech. rep., Argonne National Laboratory, 1977.

[14] J. H. Ferziger, *Numerical Methods for Engineering Application*. John Wiley and Sons, Inc., New York, NY, 1998.

[15] B. Gear, "Backward differentiation formulas," vol. 2, no. 8, p. 3162, 2007. revision 91024.

[16] L. R. J. M. Franco, I Gómez, "Sdirk methods for stiff odes with oscillating solutions," *Journal fo Computational and Applied Mathematics*, vol. 81, pp. 197–209, 1997.

[17] W. T. V. B. P. F. William H. Press, Saul A. Teukolsky, *Numerical Recipes in C: The Art of Scientific Computing*. Cambridge University Press, 1992.

[18] L. Hageman and J. Yasinsky, "Comparison of alternating direction time differencing method with other implicit method for the solution of the neutron group diffusion equations," *Nucl. Sci. Eng.*, vol. 38, pp. 8 – 32, 1969.

APPENDIX A

FIRST APPENDIX

Text for the Appendix follows.

APPENDIX B

A SECOND APPENDIX WHOSE TITLE IS MUCH LONGER THAN THE FIRST

Text for the Appendix follows.

B.1 Appendix Section

B.2 Second Appendix Section